

Cite this: *RSC Adv.*, 2015, 5, 58669

## V-containing ZrO<sub>2</sub> inorganic yellow nano-pigments†

José Miguel Calatayud, Pablo Pardo and Javier Alarcón\*

In this work we report new results on the preparation, characterization and color properties of the inorganic yellow nano-pigmenting system based on monoclinic V–ZrO<sub>2</sub> solid solution nanoparticles. The series of solid solution nanopowders were obtained by a polyol technique where the precipitates, obtained after heating at 180 °C ethylene glycol solutions of vanadyl acetate and zirconium *n*-propoxide, were annealed at different temperatures up to 1300 °C for a short duration, in order to improve their crystallinity and control the crystalline form of the final nanoparticles. On annealing at around 450 °C highly crystalline tetragonal V-containing zirconia particles were developed, which transform into the monoclinic form of the V–ZrO<sub>2</sub> solid solution after subsequent annealing at 800 °C. Interestingly, the final non-aggregated, well-shaped monoclinic zirconia solid solution particles heated even at as high temperatures as 1000 °C, were sized in the nanometric range displaying well-defined faces and edges. The chromatic coordinates of the prepared nano-pigments after annealing at different temperatures between 800 and 1300 °C indicated yellowness values comparable to conventionally prepared micrometric yellow pigments. The stability of the nano-pigments in aqueous dispersions estimated by zeta potential measurements was good with a low degree of particle aggregation. The used polyol-mediated synthesis can be up-scaled on an industrial level in the preparation of zirconia-based nano-pigmenting systems.

Received 11th May 2015  
Accepted 29th June 2015

DOI: 10.1039/c5ra08762g

[www.rsc.org/advances](http://www.rsc.org/advances)

## 1. Introduction

V–ZrO<sub>2</sub> is a well-known and widely-used ceramic pigmenting system included in the classification of mixed-metal-oxide inorganic pigments.<sup>1</sup> Furthermore, V-containing ZrO<sub>2</sub> materials are used as catalysts for different processes in which organic compounds are transformed into others which can be used as raw materials for many commercial products.<sup>2</sup> More recently, other potential applications, such as chemical sensors and electrocatalyzers, have been proved.<sup>2–4</sup> Regarding the ceramic pigmenting system, several authors have reported results on fundamental knowledge since at least 20 years ago.<sup>5–8</sup>

More recently and by using methods of preparation of solids which allow the fast progress of the reaction to the final products, its nature and mechanism of formation was described.<sup>9–11</sup> It was then confirmed that this pigment is a solid solution of vanadium in monoclinic zirconia as indicated by the results obtained on the lattice parameter variation with increasing the amount of nominal vanadium in a set of samples prepared by the sol–gel technique.<sup>11</sup> Likewise, it was demonstrated that the V cation is mainly in the oxidation state +4 replacing Zr(IV) in the

monoclinic zirconia lattice. It can be assumed, therefore, that a reasonable comprehension on the structural features of this ceramic pigment exists already. However, the microstructural control of this ceramic pigmenting system was not entirely achieved by the sol–gel technique method of preparation used due to particles' aggregation and large particle size distribution is formed.

Currently, a technological change is taking place in the ceramic pigment industry, since new decorating methodologies are being incorporated to the ceramic industry. The new methodologies are based on the use of stable dispersions of colloidal ceramic pigment particles, which by the ink-jet technology allows a digital decoration. Thus, from some years ago, the new challenge for the ceramic pigmenting science is to obtain the traditional widely-used or new pigments in the form of nanoparticles, which need to be stable in aqueous and/or other media dispersions. Since the prepared V–ZrO<sub>2</sub> ceramic pigmenting system by conventional techniques is still extensively used in the ceramic industry, it seems interesting to outline its preparation by techniques that not only allow to reach high reactivity but also the control of particle size below 100 nm and the narrowing of its particle size distributions. Furthermore, the availability of a new yellow basic color especially when the quadrichromy process is used could allow developing saturated colors over the range of firing temperatures between 800 and 1200 °C.

University of Valencia, Department of Inorganic Chemistry, Calle Doctor Moliner 50, 46100-Burjasot, Valencia, Spain. E-mail: [javier.alarcon@uv.es](mailto:javier.alarcon@uv.es)

† Electronic supplementary information (ESI) available. See DOI: 10.1039/c5ra08762g



The polyol technique has been used for the preparation of a large variety of solids at the nanoscale level. One of the key-features of this synthetic procedure is its suitability for the preparation of monodisperse and non-agglomerated particles. In the last decade this technique has been widely used for the preparation of metal particles as well as a large variety of multicomponent oxides, phosphates, sulfides and halogenides.<sup>12–17</sup> Moreover, the doping of different host lattices has been also achieved by using the polyol technique.<sup>18,19</sup>

The aim of the present paper is to report on the preparation, characterization and optical properties of well-shaped, non-aggregated V-doped ZrO<sub>2</sub> nanoparticles prepared by using a polyol technique as the method of synthesis. Since a subsequent annealing at different temperatures is required to improve the crystallinity and stabilize the monoclinic zirconia structure of the final V-ZrO<sub>2</sub> nanoparticles, their further growth and/or aggregation on annealing must be avoided. The dispersability of the obtained nanoparticles in aqueous media will be also assessed. Finally, the comparison of the structural and spectroscopic results on the polyol-mediated synthesized V-doped ZrO<sub>2</sub> nanoparticles with the ones previously reported will allow us to confirm the previously proposed mechanism of formation and other described features of this V-containing ZrO<sub>2</sub> nano-pigmenting system.

## 2. Experimental procedure

### 2.1 Synthesis of samples

Samples with stoichiometry V<sub>x</sub>Zr<sub>1-x</sub>O<sub>2</sub> and compositions in the range 0 ≤ x ≤ 0.1 were prepared by the so-called polyol method. The synthetic procedure to prepare 5 grams of final V<sub>x</sub>Zr<sub>1-x</sub>O<sub>2</sub> was as follows. The required amount of zirconium *n*-propoxide (Zr(OC<sub>3</sub>H<sub>7</sub>)<sub>4</sub>, ZnP, from Aldrich) was solved in a mixture of acetylacetone (acac) and ethylene glycol (EG). Vanadyl acetylacetonate (VO(O<sub>2</sub>C<sub>5</sub>H<sub>7</sub>)<sub>2</sub>, VOacac, from Merck), and water were added to that solution to reach the ZnP : acac : H<sub>2</sub>O molar ratio of 1 : 0.15 : 10. The concentration of all V<sub>x</sub>Zr<sub>1-x</sub>O<sub>2</sub> samples in the final solution was 0.1 M. The solution containing all the reagents was then heated at 180 °C for 2 h. The vanadium-containing zirconium solutions were light green whereas the solution with only zirconium had a yellowish hue. After around 10 min at 180 °C a precipitate appeared. The final precipitate was separated by centrifugation, washed three times with ethanol and dried. In order to follow changes in the crystallinity and to determine the temperature range at which the monoclinic V-containing zirconia nanocrystals are structurally stabilized, the dried precipitates were annealed at different temperatures over the range between 400 and 1300 °C for short times.

### 2.2 Techniques of characterization

Chemical, structural and microstructural changes from V-containing ZrO<sub>2</sub> precipitates to monoclinic V-ZrO<sub>2</sub> solid solution nanoparticles were monitored by different experimental techniques.

All samples were tested by DTA/TG, using a TG-STD A thermoanalyzer model Mettler Toledo TGA/SDTA851e/LF/1600

under air atmosphere in platinum crucibles, with a heating rate of 10 °C min<sup>-1</sup> in the temperature range between 80 and 1000 °C. The reference sample used was α-Al<sub>2</sub>O<sub>3</sub>.

X-ray diffraction analysis (model D-8 Advance, Bruker) were performed using CuK<sub>α</sub> radiation. The diffractometer had 1 and 3 mm divergence and antiscattering slits respectively, and a 3° 2θ range Lynxeye linear detector. The diffractograms were run with a step size of 0.02° 2θ and a counting time of 0.2 s. Crystalline structures were refined with the Rietveld technique, by using X'Pert Highscore Plus software, on diffractograms acquired from 5 to 120° 2θ with a step size of 0.02° 2θ and an accumulated counting time of 2 s. The refinement was started using the P2<sub>1</sub>/c space group and structure parameters derived by Winterer *et al.* (ICSD 00-37-1484). The crystallite size of samples annealed at 800 °C for short time was also determined by using the X'Pert Highscore Plus software and LaB<sub>6</sub> as standard.

Infrared absorption (IR) spectra (Model 320 Avatar, Nicolet) were obtained in the range 2000–400 cm<sup>-1</sup> using the KBr pellet method.

Micro-Raman spectra of annealed samples were obtained by means of an iHR320 Yvon Horiba model and a YAG laser at 532 nm with maximum power of 60 mW. The samples were measured in backscattering geometry at room temperature. A 50× microscope objective was used to focus the excitation laser on the sample and collect the scattered light to the spectrometer. More than 3 different areas were analysed per sample, to obtain representative results. Exposure time, number of acquisitions and laser power varied among 5–30 s, 3–10 and 30–60 mW, respectively. Data acquisition was carried out with the LabSpec software packages from Jobin Yvon.

UV-vis diffuse reflectance (DR) spectra of the specimens (Model V-670, Jasco) were obtained using the diffuse reflectance technique in the range of 200 to 2500 nm. *L*\**a*\**b*\* parameters of representative specimens were measured with the same spectrophotometer using a standard lighting C, following the CIE-*L*\**a*\**b*\* colorimetric method recommended by the CIE (Commission Internationale de l'Eclairage). In this colour system, *L*\* is the colour lightness (*L*\* = 0 for black and 100 for white), *a*\* is the green (–)/red (+) axis, and *b*\* is blue (–)/yellow (+) axis.

The microstructure of the as-precipitated and thermally treated samples was determined by field emission scanning electron microscopy at 20 kV (Model S-4800, Hitachi Ltd, Tokyo, Japan). The samples were prepared by dropping a dispersion of the powders in water directly onto the holder sample. Before the examination all specimens were coated with gold/palladium in an ion beam coater. Elemental analysis using energy-dispersive X-ray spectroscopy (EDX) of the as-prepared and annealed precipitates was also obtained by the same microscope working at 20 kV.

The morphology of pure and vanadium-containing zirconia particles was also examined using transmission electron microscopy (Model 1010, Jeol Ltd, Tokyo, Japan) at an accelerating voltage of 100 kV. Samples were dispersed in water and drops of the dispersion were transferred to a specimen copper grid carrying a lacey carbon film. Image J software was used for the size measurements performed on the micrographs and the subsequent data analysis, including the generation of size distributions.



Surface characterization and colloidal stability of the different materials were evaluated through the determination of  $\zeta$ -potential in a pH range between 3 and 11 using a Zetasizer Nano ZS (Malvern Instruments) equipment. Aqueous suspensions ( $0.1 \text{ g L}^{-1}$ ) of the materials prepared by sonication (10 minutes, 150 W) were adjusted to the different pH values with NaOH and HCl and measurements were replicated three times.

### 3. Results and discussion

#### 3.1 Preparation and characterization of V-containing $\text{ZrO}_2$ precipitates

As quite different experimental conditions might be chosen in the preparation of the precipitate precursors, it is worthwhile to mention the criteria for the specific ones chosen in this work, regarding different reagents and solvents, the temperature and time of reaction and the stabilizers agents. Likewise, although not the main topic of this work, the initial precipitates, as precursors of the products of interest, deserve a detailed study in order to better understanding the features of the final materials. What follows next, therefore, are the comments on the experimental conditions used to prepare the precipitate precursors and the description of the results of the application of the characterization techniques on those precursor products.

The most commonly used solvent in the polyol-mediated approach for the preparation of nanometric crystalline solids is EG. On increasing the hydrocarbon chain length, *i.e.* diethylene glycol (DEG), triethylene glycol (TREG), *etc.*, polyols possess higher viscosity and over reducing power relative to EG. Moreover EG was chosen as solvent in our synthesis since it is also useful to facilitate the stabilization of  $\text{V}^{4+}$  in the first stage of reaction. The preliminary study of the most suitable type of precursor as well as the concentration of precursors and the temperature and duration of the reaction is compulsory in order to get particles with well-defined size and shape for each compound. From our preliminary assays, it was concluded that for the  $0.1 \text{ M V}_x\text{Zr}_{1-x}\text{O}_2$  solution, suitable precipitates were obtained for all compositions after keeping 2 hours at  $180^\circ\text{C}$  when EG was used. On the contrary, when using DEG as solvent in the preparation of undoped  $\text{ZrO}_2$ , the obtained translucent dispersion was long time stable and no precipitate could be separated by centrifugation at 8000 rpm for 2 h. This behavior could be attributed to the precipitation of smaller particles on using DEG than EG.

It is to be noted that different effects of polyols on the particle size and dispersability of nanoparticles of distinct nature have been reported in the literature.<sup>20,21</sup> Thus, for instance, Cai and Wan reported that in the preparation of magnetite nanoparticles by the polyol technique the morphology of the reaction product is quite different depending on the characteristics of the polyol used: EG, DEG, TREG (triethylene glycol) and TTREG (tetraethylene glycol).<sup>20</sup> In this case only TREG yields non-agglomerated magnetite nanoparticles with uniform shape and narrow size distribution. Likewise, Wang *et al.*, reported the preparation of Ag nanocubes with controlled lengths below 30 nm by using DEG as solvent.<sup>21</sup> In this case, the alternative use of EG or polyols with longer

hydrocarbon chains (TEG or TREG) only led to the formation of twinned particles with irregular shapes.

In order to obtain information on the nature of the processes leading to the obtained yellow and green precipitates after heating the starting mixtures of reagents at  $180^\circ\text{C}$  for 2 h, the series of precipitates were characterized by different techniques. The elemental analysis by EDX was done to confirm that both metals, Zr and V, were present in all doped samples. Fig. 1S<sup>†</sup> displays the EDX spectra for all the prepared precipitates. A decrease of the Zr : V intensity ratio with the increasing of the nominal amount of vanadium can be inferred. The XRD patterns of the obtained precipitates in the full range of nominal compositions did not show any sharp peak, as can be observed in Fig. 2S.<sup>†</sup> However, a very broad, weak diffraction peak centered at  $2\theta$  value of around  $30^\circ$  can be distinguished in the pattern traces, possibly associated with the presence of a small fraction of nanocrystalline tetragonal and/or cubic zirconia in the precipitates. The formation of metal glycolates by reaction of metal alkoxides and EG has been reported in previous works.<sup>22,23</sup> The XRD patterns of different glycolates showed a striking similarity in the emergence of diffraction peaks, especially those located at low angle ( $\sim 12^\circ$ ),<sup>22,23</sup> not detected in the present study. Presence of zirconium glycolate is then discarded in the final precipitates. The IR spectra of precipitates shown in Fig. 3S<sup>†</sup> allow us to identify the functional groups on the surface of the precipitates. All the IR spectra were similar and beard a strong resemblance to the corresponding to EG.<sup>24</sup> This observation could confirm the role played by the EG, mainly as stabilizer of the precipitate surface avoiding agglomeration.

The aforementioned results seem to indicate that the presence of acac prevented the formation of glycolates and that the  $\text{Zr}(\text{OR})_{4-x}(\text{acac})_x$ , formed in the starting mixture of EG and acac and the VOacac, suffered hydrolysis and condensation on heating in the high-boiling point EG solvent, thus controlling the nucleation and growth of nanoparticles.

The V- $\text{ZrO}_2$  precipitates obtained with EG were relatively amorphous; nevertheless the aim of this work is to obtain highly crystalline nanoparticles, because the non-crystalline form directly affects both the energy splitting of the d-orbitals in the case of an absorption process originating from d-d transitions and, most crucial, the stability of the chromophore-containing phase, which decreases dramatically. The only way to stabilize the structural and chromatic characteristics of the V- and Zr-containing precipitates is to anneal those precipitates at different temperatures for short times, whereas avoiding aggregation of the crystalline nanoparticles. To design that annealing process, the compositional changes of the precipitates associated with that heating were followed by TG and DTA. The TG and DTA of the precipitates were similar for the different compositions, therefore only graphs corresponding to the samples  $\text{V}_{0.05}\text{Zr}_{0.95}\text{O}_2$  and  $\text{V}_{0.1}\text{Zr}_{0.9}\text{O}_2$  are shown in Fig. 4S and 5S,<sup>†</sup> respectively. TG graphs show rapid change in mass loss of around 45% in three steps for all samples. DTA showed an endothermic peak around  $100^\circ\text{C}$ , associated to the loss of physisorbed water molecules, an exothermic peak at around  $300^\circ\text{C}$  coupled with a strong mass loss that is ascribed to the



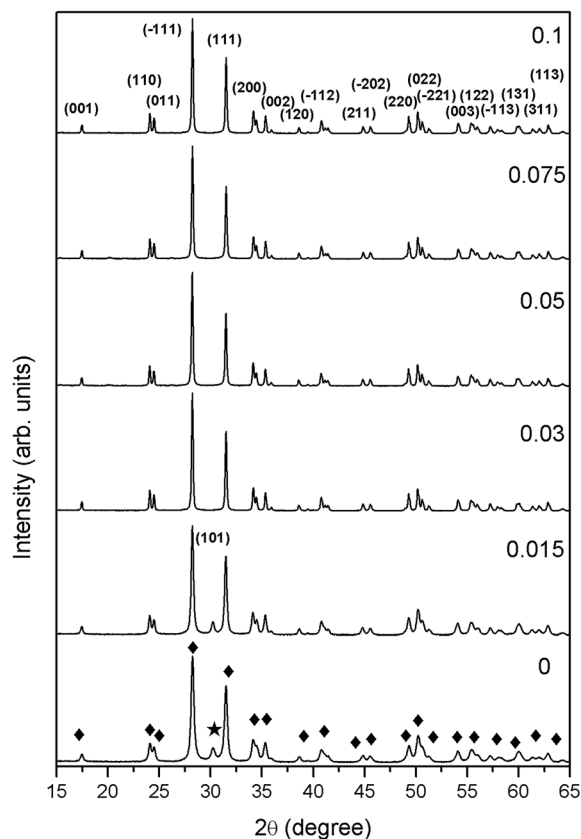


Fig. 1 XRD patterns of  $V_xZr_{1-x}O_2$  precipitates annealed at 800 °C for 3 h prepared by using EG as solvent. ★ is tetragonal zirconia and ◆ is monoclinic zirconia.

oxidation of EG, an exothermic peak at around 400 °C attributed to the crystallization of tetragonal  $V_xZr_{1-x}O_2$  solid solution and finally an exothermic peak at around 600 °C associated with the phase transition from the tetragonal  $V_xZr_{1-x}O_2$  to the monoclinic  $V_xZr_{1-x}O_2$  solid solution. From the above results the starting annealing temperature to process the obtained  $V_xZr_{1-x}O_2$  precipitates was 400 °C.

### 3.2 Structural evolution of the precipitates up to the formation of monoclinic V-containing $ZrO_2$ nanoparticles

The obtained dried precipitated powders in the EG solution were annealed at different temperatures up to 1300 °C in order to improve their crystallinity and establish the range of temperature and compositions to which each zirconia crystalline form is stable. Fig. 6S and 7S† show the XRD patterns of pure zirconia  $ZrO_2$  and vanadium-doped  $ZrO_2$  with nominal composition  $V_{0.1}Zr_{0.9}O_2$ , the sample of the prepared series with the highest content of vanadium, both annealed at different temperatures up to 1300 °C for 3 h. As it can be seen there are no large differences in the evolution of crystalline phases with the temperature. In general, for all samples annealed at 400 °C the XRD powder patterns display a set of diffraction peaks that can be indexed as corresponding to the tetragonal  $ZrO_2$  phase (ICSD 01-088-1007). This tetragonal form is detected as the only crystalline phase after annealing the samples over the range of temperatures between 400° and 500 °C. On increasing that temperature up to 800 °C the XRD patterns of all annealed precipitates can be indexed as a mixture of tetragonal and monoclinic zirconia (ICSD 00-037-1484) phases. At higher annealing temperatures than 800 °C and up to 1300 °C, the set

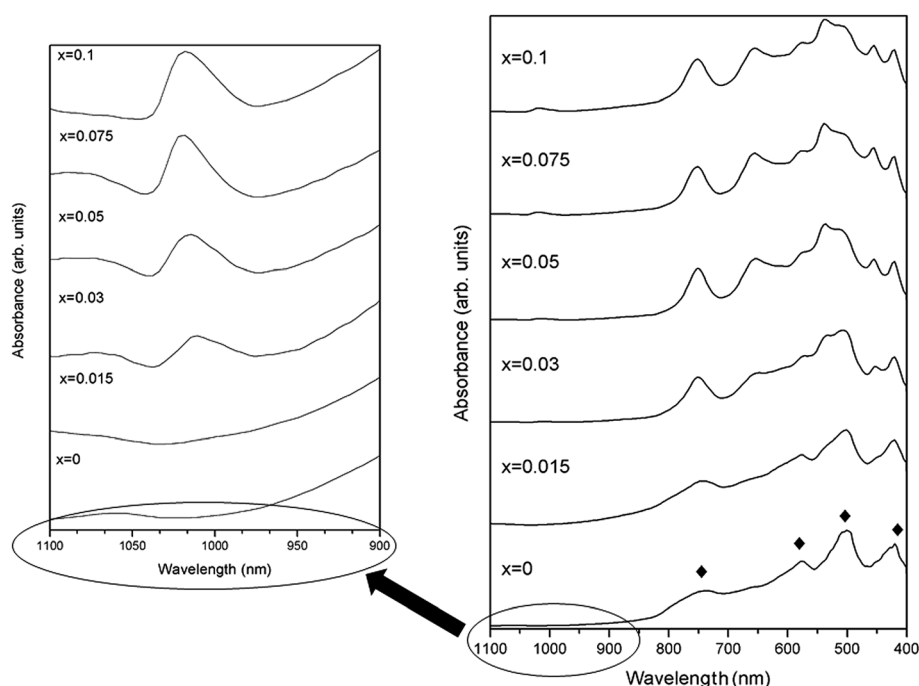


Fig. 2 (a) IR spectra of  $V_xZr_{1-x}O_2$  precipitates prepared by using EG as solvent after annealing at 800 °C; (b) zoom displaying the IR spectra in the range between 900 and 1100 nm. ◆ are bands corresponding to monoclinic zirconia.





of peaks are indexed as corresponding to a phase with the structure of monoclinic zirconia. Fig. 1 displays the XRD patterns of all samples  $V_xZr_{1-x}O_2$  in the series of compositions annealed at 800 °C for 3 h.

On comparing the results in the evolution of samples with compositions  $V_xZr_{1-x}O_2$  prepared by a conventional sol-gel method using ethanol as solvent with those obtained by the polyol method using EG annealed at similar temperatures, the only detected difference is the stabilization of phases displaying

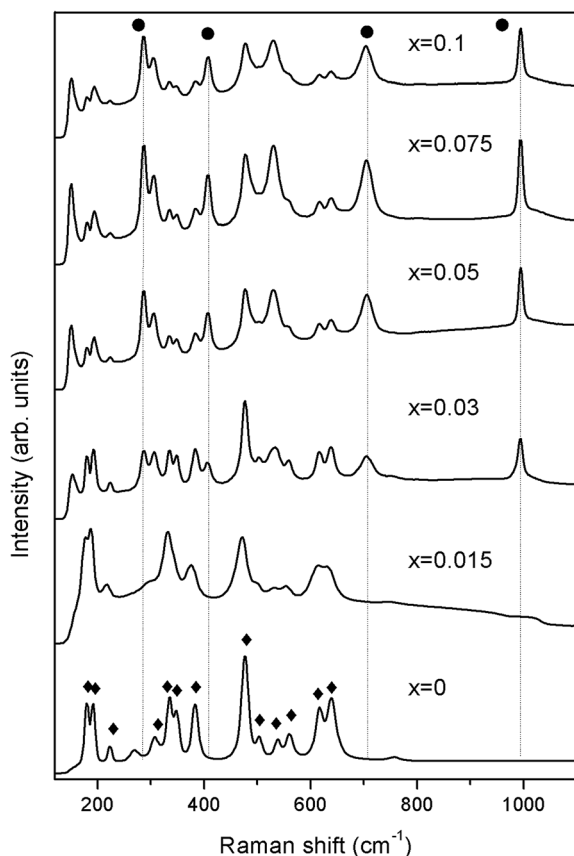


Fig. 3 Raman spectra of  $V_xZr_{1-x}O_2$  precipitates prepared by using EG as solvent after annealing at 800 °C, ◆ is monoclinic  $V_xZr_{1-x}O_2$ , ● is V=O bond.

the structure of the monoclinic zirconia at slightly lower temperature, i.e. at around 700 °C, in samples prepared by the conventional sol-gel method.

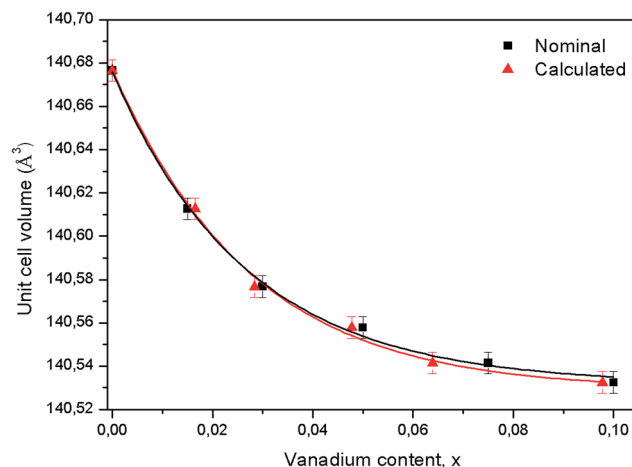


Fig. 4 Lattice volume of precipitates  $V_xZr_{1-x}O_2$ , prepared by using EG as solvent after annealing at 800 °C for 3 h, against the nominal and calculated by Rietveld refinement vanadium content  $x$ .

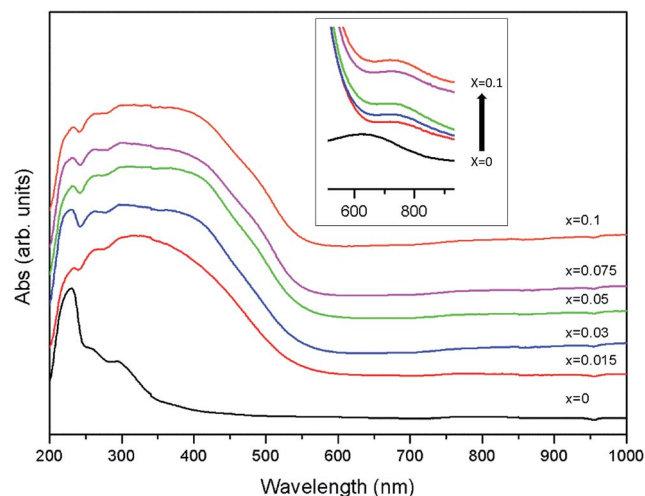


Fig. 5 UV-vis diffuse reflectance spectra of precipitates  $V_xZr_{1-x}O_2$ ,  $0 \leq x \leq 0.1$ , prepared by using EG as solvent after annealing at 800 °C for 3 h. Inset samples annealed at 1300 °C.

Table 1 Crystallographic data and details of the Rietveld refinement of monoclinic  $V_xZr_{1-x}O_2$  nano-pigments after annealing their precipitates at 800 °C for 3 h

Sample	$x = 0$	$x = 0.015$	$x = 0.03$	$x = 0.05$	$x = 0.075$	$x = 0.1$
$a$ (Å)	5.1478 (1)	5.1459 (1)	5.1446 (1)	5.1442 (1)	5.1439 (1)	5.1439 (1)
$b$ (Å)	5.2014 (1)	5.1995 (1)	5.2059 (1)	5.2059 (1)	5.2065 (1)	5.2064 (1)
$c$ (Å)	5.3214 (1)	5.3227 (1)	5.3170 (1)	5.3169 (1)	5.3159 (1)	5.3157 (1)
$\beta$ (°)	99.138 (2)	99.124 (1)	99.186 (1)	99.193 (1)	99.199 (1)	99.195 (1)
$V$ (Å³)	140.676 (5)	140.613 (5)	140.577 (5)	140.558 (5)	140.541 (5)	140.532 (5)
Zr (%)	1	0.973 (5)	0.953 (7)	0.939 (5)	0.927 (5)	0.895 (8)
V (%)	0	0.016 (5)	0.028 (7)	0.048 (5)	0.064 (5)	0.098 (8)
$R_{exp}$	2.75	2.78	2.73	2.76	2.80	2.77
$R_{wp}$	4.33	4.41	5.12	5.20	5.49	5.18
GoF	2.47	2.51	3.51	3.54	3.85	3.51



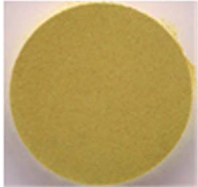





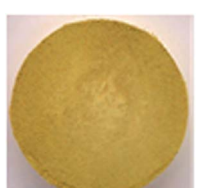

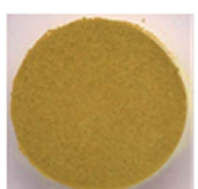



In order to prove the presence of monoclinic zirconia and while discarding the presence of cubic and/or tetragonal zirconia crystalline forms in the final samples, IR and Raman spectra of annealed samples with increasing nominal vanadium load, in the series annealed at 800 °C for 3 h are displayed in Fig. 2 and 3, respectively. As can be seen in Fig. 2a, the IR spectra of annealed  $V_xZr_{1-x}O_2$  displayed bands at 419, 502, 575 and 746  $cm^{-1}$  which can be associated with active modes in monoclinic zirconia phase.<sup>25</sup> The additional band also detected at 1015  $cm^{-1}$ , can be attributed to V=O stretching vibrations.<sup>26</sup>

The Raman spectra of these samples showed in Fig. 3, displayed bands at 180, 191, 223, 307, 334, 347, 383, 476, 503, 538, 560, 616 y 640  $cm^{-1}$ , which have been attributed to different Raman active modes in monoclinic zirconia.<sup>27–29</sup> Interestingly, four characteristic new bands at 286, 406, 706 and 991  $cm^{-1}$  appeared in all doped samples. These bands were already reported in the literature for V-doped zirconia samples prepared by sol-gel, were assigned to V=O bonds.<sup>30</sup>

From the results of the abovementioned experimental techniques, these V-containing  $ZrO_2$  nanoparticles prepared by the

**Table 2** Chromatic coordinates of monoclinic  $V_xZr_{1-x}O_2$  nano-pigments after annealing at 800 °C and 1300 °C for 3 h

Sample		800 °C		1300 °C	
$x = 0$	<i>L</i>	101.01		88.49	
	<i>a</i>	−0.29		−0.78	
	<i>b</i>	2.01		−1.71	
$x = 0.015$	<i>L</i>	80.06		73.61	
	<i>a</i>	0.25		8.16	
	<i>b</i>	34.34		46.71	
$x = 0.03$	<i>L</i>	79.18		73.03	
	<i>a</i>	1.8		7.18	
	<i>b</i>	39.39		48.13	
$x = 0.05$	<i>L</i>	78.27		70.65	
	<i>a</i>	3.39		7.87	
	<i>b</i>	43.32		48.87	
$x = 0.075$	<i>L</i>	79.7		65.5	
	<i>a</i>	3.17		7.88	
	<i>b</i>	44.12		48.5	
$x = 0.1$	<i>L</i>	75.17		63.16	
	<i>a</i>	2.63		8.69	
	<i>b</i>	40.35		46.45	



polyol technique and annealed at 800 °C for short time periods display unequivocally the structure of monoclinic zirconia.

### 3.3 Characterization of monoclinic V-containing ZrO<sub>2</sub> solid solution nanoparticles

Once the monoclinic form of the V–ZrO<sub>2</sub> solid solutions is reached after annealing over a range of temperature the follow-up step is their characterization. Several parameters are important in order to evaluate the extension of the solid solution and mechanism of formation as well as some of their specific properties such as microstructural features and optical properties. These characteristics are valuable not only for the specific application as nano-pigment but for a large number of potential applications, such as catalysts, photocatalysts and electrocatalysts.

**3.3.1. Mechanism of formation of monoclinic V<sub>x</sub>Zr<sub>1-x</sub>O<sub>2</sub> solid solution from the precipitates.** The results from the phase identification in XRD data indicate that certain amount of vanadium was present in the monoclinic zirconia-based materials obtained after annealing the precipitates obtained by the polyol *via* at 800 °C. At this point, it is worthwhile to check the change in the zirconia lattice on increasing the nominal amount of vanadium in the starting precipitate. The lattice parameters and details of the Rietveld refinement of V<sub>x</sub>Zr<sub>1-x</sub>O<sub>2</sub> precipitates annealed at 800 °C for 3 h are displayed in Table 1. Also in Fig. 4 the variation of lattice volume against the vanadium occupancy obtained in the Rietveld refinement is depicted. The lattice volume decreased almost monotonically with the increase of the nominal amount of vanadium. This result is in agreement with previously reported ones for this pigmenting system prepared by the sol–gel *via*.<sup>9,11</sup> Thus, from these results can be confirmed that on the whole range of nominal compositions up to  $x = 0.1$ , solid solutions of monoclinic V-containing ZrO<sub>2</sub> with increasing vanadium contents are obtained. As previously stated, this variation can be understood assuming that a structural cation in the monoclinic zirconia structure is substituted by a smaller one; *i.e.* the zirconium cation is replaced by vanadium (as V<sup>4+</sup> and/or V<sup>5+</sup>).<sup>11</sup> Obviously, the mechanism including the incorporation into the structure of V<sup>5+</sup> would also include some kind of electroneutrality process, either cation vacancy or interstitial anions.

**3.3.2. Optical properties of monoclinic V-containing ZrO<sub>2</sub> nanoparticles.** The UV-vis diffuse reflectance (DR) spectra of the precipitates annealed at 800 °C prepared by using EG as solvent are shown in Fig. 5. Two main features are worth mentioning in the spectra of V-containing samples: a strong band centred at around 400 nm and a weak, wide band peaked at around 750 nm. This weak band is clearly evidenced in the inset of Fig. 5, corresponding to the series of samples annealed at higher temperature, *i.e.* 1300 °C for short time, in order to do them more distinguishable. The assignment of these bands has been previously suggested by different authors.<sup>7,9</sup> Basically, the intense band encompassing the range between 200 and 300 nm can be associated with a charge transfer mechanism which, in the undoped sample, was considered to be a convolution of at least three components.<sup>7</sup> The stronger and wider absorption

displayed by all the doped samples in the range over 300 and 600 nm bears a resemblance to that showed for some V(IV) compounds such as V(OBut)<sub>4</sub>.<sup>31</sup> Finally, the weak band at around 750 nm can be associated with a d–d transition. The presence of vanadium in a lower oxidation state than +5 in the precipitate must be favoured by the reducing character of polyols. Since EG has the stronger reducing power among the polyols due to its shorter hydrocarbon chain, it must favour the presence of vanadium as V<sup>4+</sup> or lower oxidation state in the precipitate. However, it seems quite difficult to maintain lower oxidation than +4 after annealing in air at relatively high temperature.

The evolution with vanadium content of the  $L^*a^*b^*$  parameters of samples annealed at 800 °C for 3 h in the series of samples, is shown in Table 2. Also, for the sake of comparison the colorimetric parameters of a conventional vanadium–zirconia pigmenting system are shown in Table 3.<sup>32,33</sup> In all V-doped zirconia, those parameters correspond to a yellowish colour, the intensity of which increased on raising the vanadium content up to the specimen with nominal composition V<sub>0.075</sub>Zr<sub>0.925</sub>O<sub>2</sub>. For larger vanadium contents than  $x = 0.075$ , the  $b^*$  parameter decayed. An opposite trend was observed for the parameter  $a^*$ , whose minimum value was obtained for specimen with  $x = 0.03$ .

**3.3.3. Microstructural characteristics of solid solution nanoparticles.** TEM micrographs of the series of samples prepared by the polyol technique using EG as solvent with

Table 3 Chromatic coordinates of conventional yellow pigmenting systems from several references

(Zr,V)O <sub>2</sub> (ref. 32)	$L$	70.11	(Zr,Pr)O <sub>2</sub> (ref. 33)	$L$	76.8
	$a$	6.48		$a$	0.1
	$b$	45.45		$b$	55.8
(Zr,V)O <sub>2</sub> (ref. 33)	$L$	66.7	(Ti,Ni,Sb)O <sub>2</sub> (ref. 33)	$L$	79.5
	$a$	4.9		$a$	−3.2
	$b$	45.8		$b$	49.8

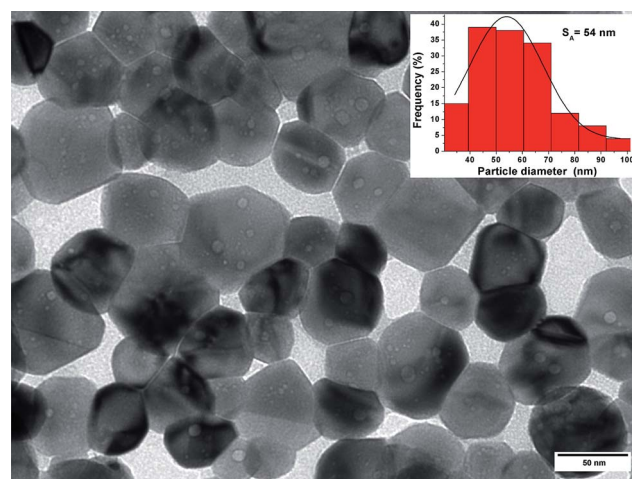


Fig. 6 TEM micrograph of monoclinic V<sub>0.015</sub>Zr<sub>0.985</sub>O<sub>2</sub> nanoparticles prepared using EG as solvent and after annealing the precipitate at 800 °C for 3 h.





subsequent annealing at 800 °C are shown in Fig. 6 to 8. It can be seen that, in general well-shaped nanoparticles sized in the range between 50 and 120 nm are obtained. The main diameter deduced *via* statistical evaluation of 150 particles of each sample is shown in Table 4. Also the particle size distribution of the corresponding samples is shown as an inset in Fig. 6 to 8. As it can be inferred from Table 4 the mean size of the monoclinic  $V_xZr_{1-x}O_2$  samples increased with the entry of dopant into the

zirconia lattice up to  $x = 0.03$  but remained almost constant on increasing the amount of dopant up to  $x = 0.1$  in the series of samples. It is also to note that the particle size distribution experienced a slight broadening with the dopant content as can be detected in the insets of Fig. 6 to 8. SEM micrographs of the samples confirmed the microstructure displayed by TEM micrographs as can be seen in Fig. 9 to 11. Furthermore, well-defined crystalline habits displaying flat faces can be clearly distinguished in SEM micrographs. To evidence the presence of V in the precipitate annealed at 800 °C, elemental analysis by EDX was performed. The spectra shown in Fig. 8S† confirm the

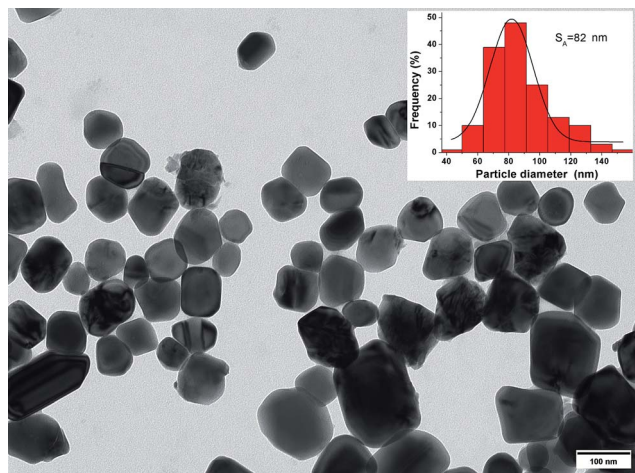


Fig. 7 TEM micrograph of monoclinic  $V_{0.05}Zr_{0.95}O_2$  nanoparticles prepared using EG as solvent and after annealing the precipitate at 800 °C for 3 h.

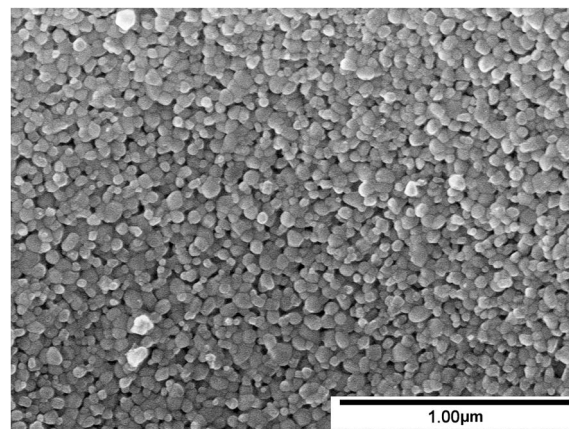


Fig. 9 SEM micrograph of monoclinic  $V_{0.015}Zr_{0.985}O_2$  nanoparticles prepared using EG as solvent and after annealing the precipitate at 800 °C for 3 h.

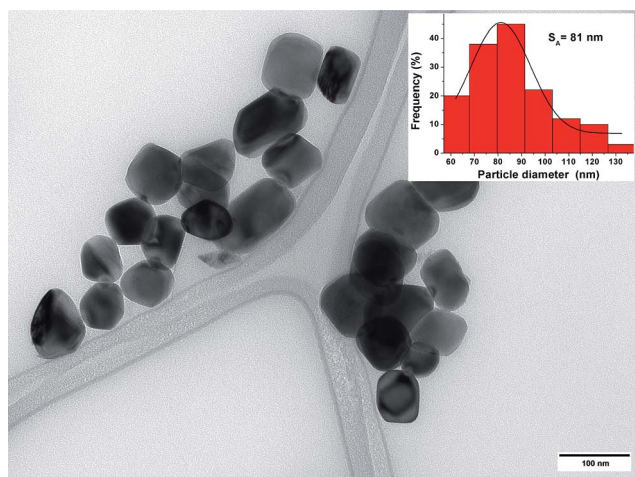


Fig. 8 TEM micrograph of monoclinic  $V_{0.1}Zr_{0.9}O_2$  nanoparticles prepared using EG as solvent and after annealing the precipitate at 800 °C for 3 h.

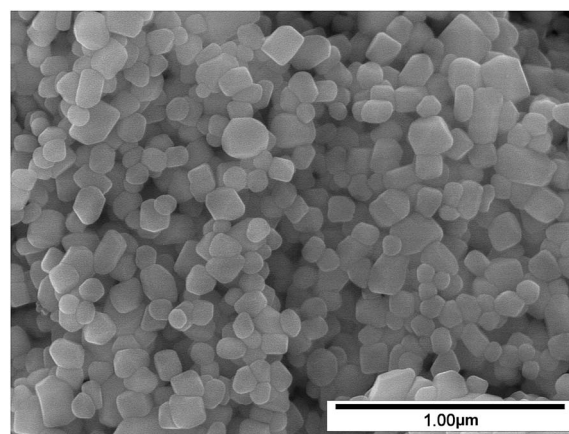


Fig. 10 SEM micrograph of monoclinic  $V_{0.05}Zr_{0.95}O_2$  nanoparticles prepared using EG as solvent and after annealing the precipitate at 800 °C for 3 h.

**Table 4** Crystallite sizes of monoclinic  $V_xZr_{1-x}O_2$  solid solutions obtained from XRD patterns (Rietveld method) and from TEM images *via* statistical evaluation of 150 particles of each sample (Image J)

	$x = 0$	$x = 0.015$	$x = 0.03$	$x = 0.05$	$x = 0.075$	$x = 0.1$
XRD patterns (nm)	29 (1)	37 (1)	65 (1)	64 (1)	65 (1)	66 (1)
TEM images (nm)	43 (2)	54 (2)	80 (2)	82 (1)	80 (5)	81 (1)





presence of V in the final monoclinic V-ZrO<sub>2</sub> nanoparticles. These results are in accordance with the formation of V-ZrO<sub>2</sub> solid solution.

An interesting parameter of nanoparticles determined from the broadening of the Bragg peaks in the XRD pattern is the crystallite size. We have determined crystallite sizes of

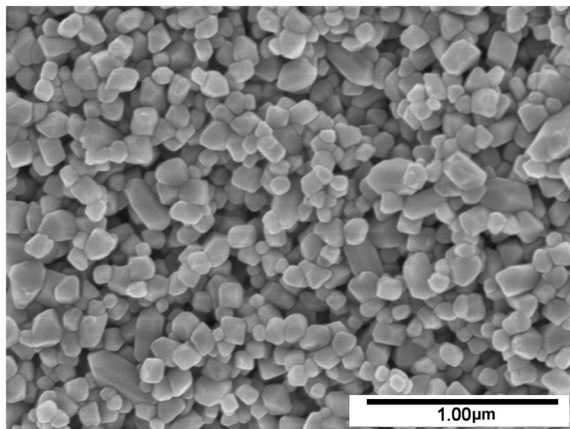


Fig. 11 SEM micrograph of monoclinic V<sub>0.1</sub>Zr<sub>0.9</sub>O<sub>2</sub> nanoparticles prepared using EG as solvent and after annealing the precipitate at 800 °C for 3 h.

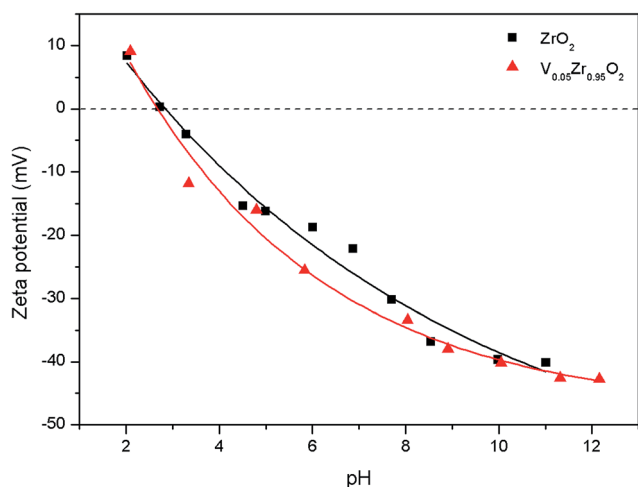


Fig. 12  $\zeta$ -potential variation of monoclinic ZrO<sub>2</sub> and V<sub>0.05</sub>Zr<sub>0.95</sub>O<sub>2</sub> nanoparticles in aqueous solution.

monoclinic V<sub>x</sub>Zr<sub>1-x</sub>O<sub>2</sub> solid solutions previously annealed at 800 °C by the Rietveld method. The corresponding values, in the range over 30 and 70 nm, are included in Table 4. As it can be observed the trend in the series was the same as the observed in the mean diameters of nanoparticles measured on TEM images. The crystallite size increased on doping up to  $x = 0.03$  and from that composition point on, remained constant. Nevertheless, in general, crystallite sizes were a bit smaller than nanoparticle sizes. That small difference between the crystallite size determined from XRD and the averaged particle diameter from TEM images is quite usual and could be due to the overestimation of sizes by measuring particle sizes in images.

#### 4. Dispersability of V-ZrO<sub>2</sub> solid solution nanoparticles

In order to check the effect of the experimental synthetic conditions on the surface properties of the monoclinic V-doped zirconia,  $\zeta$ -potential measurements of their aqueous suspensions were performed. Fig. 12 shows the pH dependence of  $\zeta$ -potential of suspensions of pure ZrO<sub>2</sub> and V<sub>0.05</sub>Zr<sub>0.95</sub>O<sub>2</sub> particles prepared by annealing the precipitate at 800 °C for 3 h. As can be seen, both samples showed low isoelectric point (IEP), *ca.* 2.5, so the doping of zirconia nanoparticles had no influence in this parameter. It is to note that the IEP was slightly under the range between 4 to 11, usually reported in the literature for different zirconia materials.<sup>34,35</sup> In general, it is assumed that a value of zeta potential above 30 mV (or under -30 mV) leads to a good stability and a small degree of particles aggregation.

#### 5. Overview of the polyol process leading to monoclinic V-ZrO<sub>2</sub> nano-pigments

Fig. 13 shows a scheme of the different steps leading to final V-containing zirconia nano-pigments displaying the structure of monoclinic zirconia, suitable for application in the ink-jet process. The first step in the process is the formation of very small particles with a certain degree of aggregation. The aggregates display sizes lower than 20 nm and constitute the final precipitate after heating the mixture of reagents in the EG (polyol). These precipitates are amorphous to the X-ray powder diffraction but as reported before seems to be made up by an

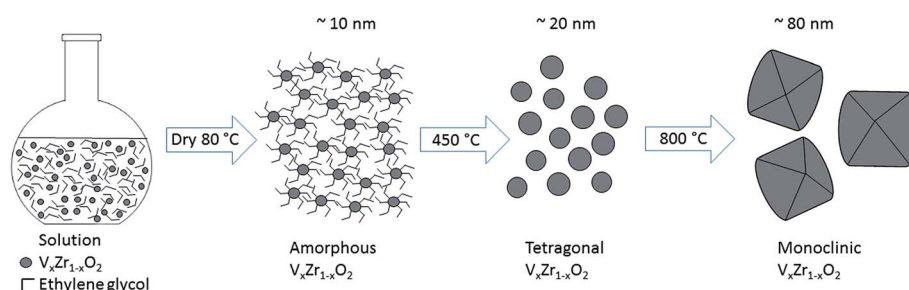


Fig. 13 Schematic graph summarizing the low-temperature polyol-mediated process leading to V-ZrO<sub>2</sub> nano-pigments.



inner crystalline nucleus and an outer amorphous coating.<sup>36</sup> After annealing at around 450 °C crystalline nanoparticles displaying the structure of tetragonal zirconia with sizes around 20 nm are formed and by further annealing at 800 °C the phase transition to the monoclinic zirconia structure takes place. It is interesting to note that final well-shaped particles sized in the range between 50 and 120 nm and with well-defined crystalline habits are developed by the present methodology.

## 6. Conclusions

Monoclinic  $V_xZr_{1-x}O_2$  solid solution nanoparticles were prepared in a wide range of compositions  $0 \leq x \leq 0.1$  by the polyol approach using EG as solvent. Moreover, the EG played an additional role as stabilizing agent of nanoparticles by limiting particle growth and almost preventing agglomeration. After annealing the precipitates at temperatures of 800 °C, morphologically well-defined monoclinic V-ZrO<sub>2</sub> solid solution nanoparticles with sizes encompassing the range between 50 and 120 nm were obtained.

The chromatic coordinates of the prepared nano-pigments after annealing at different temperatures between 800 and 1300 °C indicated yellowness values comparable to conventionally prepared micrometric yellow pigments. The stability of the nano-pigments in aqueous dispersions estimated by zeta potential measurements was good and a small degree of particles aggregation occurred.

The use of the polyol-mediated synthesis allowed the preparation of V-containing ZrO<sub>2</sub> inorganic yellow nano-pigments by an easy procedure without requiring neither multisequential steps nor advanced experimental conditions or equipment. These characteristics allow using the polyol approach as a suitable way of industrial manufacture of nano-pigments.

From the results obtained in this specific pigmentation ceramic system it can be inferred that the polyol approach can be applied for the preparation of other widely used micrometric ceramic pigmentation systems in the nanometric scale with a good control of the three main characteristics of particles, *i.e.*, size, degree of agglomeration and phase composition.

## Acknowledgements

Financial support from the Spanish Ministry of Economy and Competitiveness through project CONSOLIDER INGENIO 2010 CSD2010-00065 is acknowledged. Technical support from the Servei Central de Suport a l'Investigació Experimental (SCSIE) of the University of Valencia in the application of TEM and XRD techniques is also acknowledged.

## References

- 1 A. Burgyan and R. A. Eppler, *Am. Ceram. Soc. Bull.*, 1983, **62**, 1001.
- 2 R. Sasikala, V. Sundarshan, T. Sakuntala, J. C. Sudakar, R. Naik and S. R. Bharadwaj, *Appl. Catal.*, A, 2008, **350**, 252.
- 3 A. Domenech and J. Alarcón, *Anal. Chem.*, 2007, **79**, 6742.
- 4 A. Domenech and J. Alarcón, *Anal. Chim. Acta*, 2002, **452**, 11.
- 5 F. T. Booth and G. N. Peel, *Trans. Br. Ceram. Soc.*, 1962, **61**, 359.
- 6 G. Monros, J. Carda, M. A. Tena, P. Escribano and J. Alarcón, *Trans. Br. Ceram. Soc.*, 1991, **90**, 157.
- 7 F. Ren, S. Ishida and N. Takeuchi, *J. Am. Ceram. Soc.*, 1993, **76**, 1825.
- 8 P. Tartaj, C. J. Serna, J. Soria and M. Ocaña, *J. Mater. Res.*, 1998, **13**, 413.
- 9 J. Alarcón, *J. Mater. Sci.*, 2001, **36**, 1189.
- 10 C. Valentín, J. V. Folgado and J. Alarcón, *Mater. Res. Bull.*, 2001, **36**, 1615.
- 11 F. J. Torres, J. M. Amigó and J. Alarcón, *J. Solid State Chem.*, 2003, **173**, 40.
- 12 J. Merikhi, H.-O. Jungk and C. Feldmann, *J. Mater. Chem.*, 2000, **10**, 1311.
- 13 C. Feldmann and H.-O. Jungk, *Angew. Chem., Int. Ed.*, 2001, **40**, 359.
- 14 C. Feldmann, *Adv. Mater.*, 2001, **13**, 1301.
- 15 C. Feldmann, *Scr. Mater.*, 2001, **44**, 2193.
- 16 C. Feldmann, *Adv. Funct. Mater.*, 2003, **13**, 101.
- 17 C. Feldmann, *Solid State Sci.*, 2005, **7**, 868.
- 18 S. D. Meetei, Sh. D. Singh and V. Sudarsan, *J. Alloys Compd.*, 2012, **514**, 174.
- 19 M. Siemons and U. Simon, *Sens. Actuators, B*, 2007, **126**, 595.
- 20 W. Cai and J. Wan, *J. Colloid Interface Sci.*, 2007, **305**, 366.
- 21 Y. Wang, Y. Zheng, C. Z. Huang and Y. Xia, *J. Am. Chem. Soc.*, 2013, **135**, 1941.
- 22 X. Jiang, Y. Wang, T. Herricks and Y. Xia, *J. Mater. Chem.*, 2004, **14**, 695.
- 23 S. N. Rishikeski, S. S. Joshi, M. K. Temgir and J. R. Bellare, *Dalton Trans.*, 2013, **42**, 5430.
- 24 C. Murli, N. Lu, Z. Dong and Y. song, *J. Phys. Chem. B*, 2013, **116**, 12574.
- 25 S. F. Wang, F. Gu, M. K. Lü, Z. S. Yang, G. J. Zhou, H. P. Zhang, Y. Y. Zhou and S. M. Wang, *Opt. Mater.*, 2006, **28**, 1222.
- 26 B. Vlčková, B. Strauch and M. Horák, *Collect. Czech. Chem. Commun.*, 1987, **52**, 686.
- 27 D. Gazzoli, G. Mattei and M. Valigi, *J. Raman Spectrosc.*, 2007, **38**, 824.
- 28 E. F. Lopez, V. S. Escribano, M. Panizza, M. M. Carnasciali and G. Busca, *J. Mater. Chem.*, 2001, **11**, 1891.
- 29 B.-K. Kim and H.-O. Hamaguchi, *Phys. Status Solidi B*, 1997, **203**, 557.
- 30 J. T. Muya, I. K. Kajimini and O. E. Kasende, *Spectrosc. Lett.*, 2014, **47**, 107.
- 31 E. C. Alyea and D. C. Bradley, *J. Chem. Soc. A*, 1969, **16**, 2330.
- 32 C. Dziubak, *Mater. Sci.-Pol.*, 2012, **30**, 398.
- 33 M. Dondi, F. Matteucci, I. Zama and G. Cruciani, *Mater. Res. Bull.*, 2007, **42**, 64.
- 34 Y. Jia, C. Duran, Y. Hotta, K. Sato and K. Watari, *J. Colloid Interface Sci.*, 2005, **291**, 292.
- 35 C. Renger, P. Kuschel, A. Kristoffersson, B. Clauss, W. Oppermann and W. Sigmund, *Phys. Chem. Chem. Phys.*, 2004, **6**, 1467.
- 36 V. G. Kessler, *J. Sol-Gel Sci. Technol.*, 2009, **51**, 264.

